

A possible mass distribution of primordial black holes implied by LIGO-Virgo

Heling Deng*

Physics Department, Arizona State University, Tempe, AZ 85287, USA

Abstract

The LIGO-Virgo Collaboration has so far detected around 90 black holes, some of which have masses larger than what were expected from the collapse of stars. The mass distribution of LIGO-Virgo black holes appears to have a peak at $\sim 30M_{\odot}$ and two tails on the ends. By assuming that they all have a primordial origin, we analyze the GWTC-1 (O1&O2) and GWTC-2 (O3a) datasets by performing maximum likelihood estimation on a broken power law mass function $f(m)$, with the result $f \propto m^{1.2}$ for $m < 35M_{\odot}$ and $f \propto m^{-4}$ for $m > 35M_{\odot}$. This appears to behave better than the popular log-normal mass function. Surprisingly, such a simple and unique distribution can be realized in our previously proposed mechanism of PBH formation, where the black holes are formed by vacuum bubbles that nucleate during inflation via quantum tunneling. Moreover, this mass distribution can also provide an explanation to supermassive black holes formed at high redshifts.

*Electronic address: heling.deng@asu.edu

I. INTRODUCTION

Over the past few years, the LIGO-Virgo Collaboration has detected gravitational waves emitted by about 50 inspiraling and merging black hole binaries [1, 2], and many more events are anticipated in the near future. It is intriguing that most of the black holes have masses $\sim 30M_\odot$, which certainly provides indicative information of the mass distribution of black holes in the universe.

The origin of these black holes is so far unknown. While the possibility that they are ordinary astrophysical black holes from stellar collapse (possibly from different channels) are under active investigations [3–6], a fascinating speculation is that LIGO-Virgo has detected primordial black holes (PBHs) [7–9]. PBHs are hypothetical black holes formed by deviations from density homogeneity in the early universe, before any large scale structures and galaxies. Their masses can range from the Planck mass ($\sim 10^{-5}$ g) to many orders of magnitude larger than the solar mass ($M_\odot \sim 10^{33}$ g). After the release of LIGO-Virgo results, much effort has been dedicated to constrain PBHs and the role they play in dark matter [9–13]. It is now generally recognized that they are unlikely to constitute all dark matter due to the small merger rate inferred by LIGO-Virgo.

It is also of great interest to constrain particular PBH mass distributions with the LIGO-Virgo results [10, 14–17]. Among them the log-normal mass function [18] is the most popular because it is a good approximation for various PBH mechanisms [19–21]. However, if all LIGO-Virgo black holes were PBHs, the peak of the log-normal function should be at $\sim 20M_\odot$, which is incompatible with what was observed. The possibility of LIGO-Virgo black holes being a mixture of two populations of black holes was recently considered in ref. [22], which concludes that astrophysical black holes that dominate the mass range $m \lesssim 15M_\odot$ together with PBHs given by a log-normal (or critical collapse) mass function are much more probable than PBHs only.

In this paper, inspired by ref. [22], we perform a maximum likelihood estimation to fit the LIGO-Virgo datasets with a broken power law only. More sophisticated techniques (e.g., Bayesian analysis [23, 24]) are available, but we believe likelihood analysis should suffice for our purposes, given the limited number of detected events and uncertainties in PBH formation. We shall also neglect some details in analyzing the formation of PBHs and binaries, as long as they are not expected to affect the results by orders of magnitude. For

instance, following ref. [22], we shall not consider the impact from black hole's spin and mass accretion.

Apart from the single peak at $\sim 30M_{\odot}$ in the distribution of LIGO-Virgo black holes, our investigation of the broken power law mass spectrum is mainly motivated by a PBH mechanism we proposed in recent years. In a series of works [25–27], we studied PBHs formed by vacuum bubbles that possibly nucleate during inflation. Depending on its size after inflation ends, a bubble will turn into a black hole in the either subcritical or supercritical regime, and the mass distributions of black holes in these two regimes could obey different power laws. We would like to know if the best-fit parameters from likelihood analysis of LIGO-Virgo data is compatible with this mechanism. Surprisingly, the broken power law mass function implied by the LIGO-Virgo black holes can indeed be realized in our model.

The rest of the paper is organized as follows. In section II, we will first discuss the merger rate of PBHs and the detection probability of LIGO-Virgo, and then apply maximum likelihood estimation to find the best-fit parameters for the broken power law mass function. In section III, we will study the mechanism of PBH formation from primordial bubbles and how could produce the LIGO-Virgo black holes. Conclusions will be summarized and discussed in section IV. We set $c = \hbar = G = 1$ throughout the paper.

II. PBHS AND LIGO-VIRGO EVENTS

It will be assumed that all black holes detected by LIGO-Virgo are primordial. They are formed during the radiation era and behave like dark matter, with their number and mass density diluted by Hubble expansion. Two neighboring black holes may collide as their gravitational attraction defeats the Hubble stretching before the radiation-dust equality. Disturbance from the surrounding environment, a typical example being a third nearby black hole exerting a tidal torque, may impede the head-on collision, leading to the formation of an inspiraling binary. If the coalescence time of the binary is comparable to the age of the universe, gravitational waves from the merger could possibly be detected when they reach the earth. Roughly speaking, whether a merger event can be heard depends on the detector's sensitivity, the masses of the two black holes (source masses), the time when the merger took place (source redshift), and the sky location and orientation of the binary system. In order to estimate how often a merger event can be recorded, we also need the merger rate of the

binaries, which is determined by the underlying mechanism of PBH formation.

A. PBH mass function and merger rate

We characterize the mass distribution of PBHs by mass function $\psi(m)$, defined by

$$\psi(m) = \frac{m}{\rho_{CDM}} \frac{dn}{dm}. \quad (1)$$

Here m is the black hole mass, dn is the number density of black holes within the mass range $(m, m + dm)$, and ρ_{CDM} is the energy density of cold dark matter. Since black holes and dark matter are diluted by cosmic expansion in the same way, $\psi(m)$ is a constant over time. Integrating $\psi(m)$ gives the total fraction of dark matter in PBHs:

$$f_{PBH} \equiv \frac{\rho_{PBH}}{\rho_{CDM}} = \int \psi(m) dm, \quad (2)$$

where $\rho_{PBH} = \int m dn$ is the energy density of PBHs. If all dark matter is made of PBHs, we have $f_{PBH} = 1$.

Another function often used to describe the PBH mass distribution is

$$f(m) \equiv m\psi(m), \quad (3)$$

which can be interpreted as the fraction of dark matter in PBHs at m within the mass range $\Delta m \sim m$. This function is particularly useful if the spectrum is relatively broad.

The PBH merger rate in the early universe is well studied in the literature [9–13]. In this paper we take the formula of differential merger rate from ref. [14]:

$$dR \approx \frac{1.6 \times 10^6}{\text{Gpc}^3 \text{yr}} f_{PBH}^{-21/37} \left(\frac{t}{t_0}\right)^{-34/37} \left(\frac{M}{M_\odot}\right)^{-32/37} \eta^{-34/37} S(\psi, f_{PBH}, M) \psi(m_1) \psi(m_2) dm_1 dm_2. \quad (4)$$

Integrating dR over all masses gives the number of merger per Gpc^3 per year. Here m_1 and m_2 are the two masses in the binary, $M \equiv m_1 + m_2$ and $\eta \equiv m_1 m_2 / M^2$; t is the time when the merger occurs, and t_0 is the present time; S is a suppression factor accounting for the effects from other matter components, including nearby black holes, and $S = \mathcal{O}(1)$ for a not particularly wide spectrum. In our calculations we shall approximate S by a simplified expression given in ref. [22], but setting $S = 1$ would not lead to much difference.

To roughly estimate the largest f_{PBH} we can have from the LIGO-Virgo results, we can assume a monochromatic mass function with $\psi(m) = f_{PBH} \delta(m - 30M_\odot)$, i.e., all PBHs have

mass $30M_\odot$. Setting $t = t_0$ and $S = 1$, we have

$$\int dR \sim 10^5 f_{PBH}^{53/37} \text{Gpc}^{-3} \text{yr}^{-1}. \quad (5)$$

The merger rate implied by LIGO-Virgo is $\mathcal{O}(10-100)\text{Gpc}^{-3}\text{yr}^{-1}$, which gives $f_{PBH} \sim 10^{-3}$. Therefore, if all PBHs are of masses around $30M_\odot$, they can at most contribute to 0.1% of the dark matter.

The distribution of LIGO-Virgo black holes is clearly not monochromatic. In this paper we shall consider the 10 black hole merger events from the GWTC-1 catalog [1] and 34 events from GWTC-2 (discarding GW190719 and GW190909) [2], so there are 88 black holes in our dataset. In fig. 1, we depict the black hole numbers in different mass ranges. The distribution appears to have a peak at $m_* \sim 30M_\odot$ and two tails on the ends, with more black holes having masses less than m_* than those on the other end. The simplest mass function that can be conceived is a broken power law,

$$\psi(m) = \frac{f_{PBH}}{m_*} (\alpha_1^{-1} - \alpha_2^{-1})^{-1} \begin{cases} (m/m_*)^{\alpha_1-1}, & m < m_* \\ (m/m_*)^{\alpha_2-1}, & m > m_* \end{cases}, \quad (6)$$

which satisfies $\int \psi dm = f_{PBH}$. We further assume $\alpha_1 > 0$ and $\alpha_2 < 0$ such that $f(m) = m\psi(m)$ has a peak at m_* , which means most contribution to the PBH energy density comes from black holes with masses around m_* . In the next subsection, we will analyze the LIGO-Virgo results and find the best-fit parameters for (6).

B. Maximum likelihood estimation

Given the differential merger rate found by eq. (4), the expected number of merger signals reaching the earth per unit time within the ranges $(m_1, m_1 + dm_1)$, $(m_2, m_2 + dm_2)$, and $(z, z + dz)$ can be evaluated as [28]

$$dN(m_1, m_2, z) = \frac{1}{1+z} \frac{dV_c}{dz} \frac{dR}{dm_1 dm_2} dm_1 dm_2 dz, \quad (7)$$

where $(1+z)^{-1}$ accounts for the time difference between the source frame and the detector frame, and V_c is the comoving Hubble volume. For later convenience, we define

$$\Lambda(m_1, m_2, z) \equiv \frac{1}{1+z} \frac{dV_c}{dz} \frac{dR}{dm_1 dm_2} \quad (8)$$

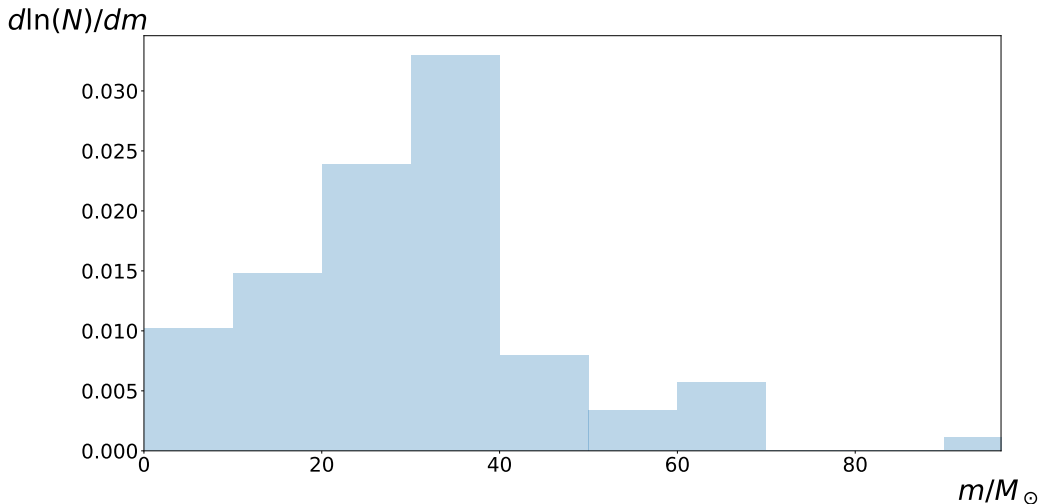


FIG. 1: Numbers of detected LIGO-Virgo black holes in different mass ranges, rescaled such that the areas add up to 1. There are 88 black holes in total. The black hole masses are simply taken to be the median values reported in refs. [1, 2]. The distribution certainly depends on the resolution of mass and the choice here is somehow arbitrary. Considering that the measurement uncertainties are $\mathcal{O}(10)M_\odot$ and that a smaller resolution would give a less clear pattern due to the insufficient number of detected events, we believe $\Delta m = 10M_\odot$ is a plausible choice.

In addition, we ought to take into account the fact that not all merger events can be observed by LIGO-Virgo. The detection probability of an event depends on the sensitivity of the instruments, the waveform of the signal as well as the extrinsic parameters of the binary system, i.e., its sky location and orientation. Integrating out the extrinsic parameters for a given detector gives its detection probability $p_{det}(r)$, with $r \equiv \rho_c/\rho(m_1, m_2, z)$. Here ρ_c is the threshold signal-to-noise ratio above which a signal can be detected, usually taken as $\rho_c = 8$; and ρ is the signal-to-noise ratio for a merger located directly above the detector. ρ is defined by

$$\rho(m_1, m_2, z) = 2\sqrt{\int \frac{|\tilde{h}(f)|^2}{S_n(f)} df}, \quad (9)$$

where $\tilde{h}(f)$ is the Fourier transform of the signal, and $S_n(f)$ is the power spectrum of the detector's strain noise. In this work, $\tilde{h}(f)$ and $S_n(f)$ are taken from refs. [22, 29] and refs. [1, 2] respectively. Then the detection probability of a particular event can be found by the parameter fit of $p_{det}(r)$ given in the appendix of ref. [28]. Since $S_n(f)$ is unique to a certain run, $p_{det}(r)$ takes different values in, e.g., O1&O2 and O3a of LIGO-Virgo.

Now the total expected number of detection during a certain run can be found by

$$N_e = T_o \int p_{det}(m_1, m_2, z) dN, \quad (10)$$

where T_o is the observation time interval (166.6 days for O1&O2 and 183.3 days for O3a). Therefore, once we are given the PBH mass function and the detector's sensitivities ($S_n(f)$), we are able to obtain from eq. (10) the expected number of observable events.

We assume that (observable) mergers occur randomly with a constant rate, so they reach the detectors following a Poisson process. Let N_o be the actual number of observed events. Then the probability of this happening during the observation interval is

$$p_{Poisson} \propto N_e^{N_o} e^{-N_e}. \quad (11)$$

The likelihood of a single detected event with source masses $m_{1,o}$, $m_{2,o}$ and redshift z_o is

$$p_o \propto \frac{p_{det}(m_{1,o}, m_{2,o}, z_o) \Lambda(m_{1,o}, m_{2,o}, z_o)}{\int p_{det}(m_1, m_2, z) dN}. \quad (12)$$

Here we have made an assumption that the source masses and redshift can be perfectly determined by detection. In practice, we take $m_{1,o}$, $m_{2,o}$ and z_o to be the median values of the posterior samples reported by LIGO-Virgo [1, 2]. In reality, their values are given with probability distributions resulting from measurement uncertainties.¹ Note that the denominator in eq. (12) is $\propto N_e$. Then the likelihood of all black hole merger events detected by LIGO-Virgo is

$$\mathcal{L} = p_{Poisson} \prod_{i=1}^{N_o} p_o^i \propto e^{-N_e} \prod_{i=1}^{N_o} p_{det}(m_{1,o}^i, m_{2,o}^i, z_o^i) \Lambda(m_{1,o}^i, m_{2,o}^i, z_o^i), \quad (13)$$

where each event is denoted by a superscript i . By maximizing the log-likelihood $\ln \mathcal{L}$ with the GWTC-1 and GWTC-2 datasets, we will be able to attain the constraints on a PBH mass function.

There are four parameters in a broken power law (6): α_1 , α_2 , m_* and f_{PBH} . Scanning through the relevant part of the parameter space, we found the largest log-likelihood $\ln \mathcal{L}_{max}$ at

$$\alpha_1 \approx 1.2, \quad \alpha_2 \approx -4, \quad m_* \approx 35 M_\odot, \quad f_{PBH} \approx 0.0013. \quad (14)$$

¹ In order to account for the measurement uncertainties, the standard approach to calculate p_o is to replace the numerator in eq. (12) by $\langle \Lambda(m_{1,o}, m_{2,o}, z_o) / \pi(m_{1,o}, m_{2,o}, z_o) \rangle$, where $m_{1,o}$, $m_{2,o}$ and z_o are the posterior samples, π is the corresponding source prior, and the brackets denote an average over all samples of that event [23, 30].

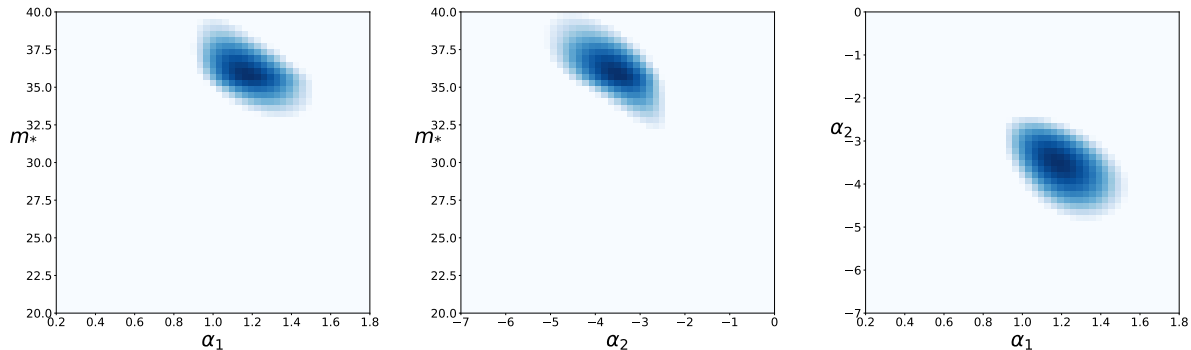


FIG. 2: Three 2-D slices of the 4-D parameter space with $f_{PBH} = 0.0013$. The darkest spot corresponds to the largest likelihood \mathcal{L}_{max} , and the shaded regions are where the parameter values give likelihoods \mathcal{L} with $\ln(\mathcal{L}_{max}/\mathcal{L}) \leq 2$. *Left:* $\alpha_2 \approx 1.2$. *Middle:* $\alpha_1 \approx -4$. *Right:* $m_* \approx 35M_\odot$. The unit for m_* is M_\odot .

These results are also partly shown in fig. 2. The power law mass function from different PBH mechanisms was discussed in, e.g., refs.[26, 31, 32], which suggested $f(m) \propto m^{-1/2}$ (for large masses). These models are obviously disfavored by LIGO-Virgo.

As a comparison, we did the same analysis for the log-normal mass function

$$\psi(m) = \frac{f_{PBH}}{m\sqrt{2\pi}\sigma} \exp\left[-\frac{\ln^2(m/m_c)}{2\sigma^2}\right]. \quad (15)$$

The most probable parameters are

$$m_c \approx 20M_\odot, \quad \sigma \approx 0.6, \quad f_{PBH} \approx 0.0013, \quad (16)$$

which are consistent with the results found in refs. [10, 14, 22, 24]. The difference between the maximum log-likelihood of broken power law and that of log-normal is $\ln(\mathcal{L}_{BPL}/\mathcal{L}_{LN}) \approx 5$. However, considering that we are evaluating the likelihood ratio with two different models, and that the broken power law has one more free parameter, we cannot say with much confidence that the broken power law is a better model at the moment in explaining the LIGO-Virgo results.

Nevertheless, using the Metropolis–Hastings algorithm, we have drawn 50000 random samples from the probability distribution $p_{det}(m_1, m_2, z)dN$ with the best-fit parameters, both for the broken power law and the log-normal model, and compared the resulting mass distributions with that from LIGO-Virgo black holes. As we can see from fig. 3, although it

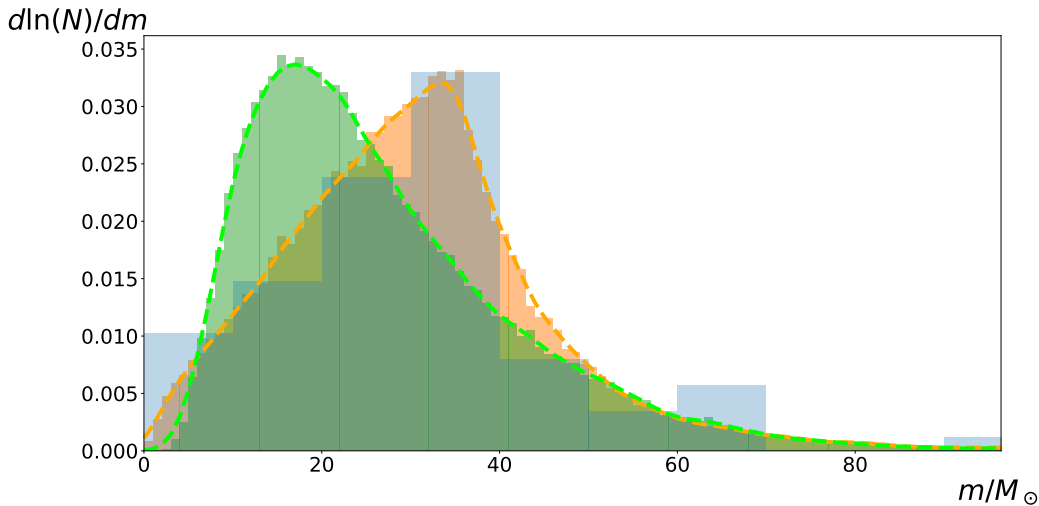


FIG. 3: Mass distributions of black holes from LIGO-Virgo (blue), the best-fit broken power law (orange) and log-normal (green).

is difficult to compare models under likelihood analysis, the broken power law mass function appears to be a better fit than the log-normal.

In the next section we will discuss a physical mechanism where PBHs could form with such a simple distribution.

III. PBHS FROM PRIMORDIAL BUBBLES

In a series of works [25–27], we studied in detail a mechanism of PBH formation where black holes are formed by vacuum bubbles that nucleate during inflation. After inflation ends, a bubble will eventually turn into a black hole in the either subcritical or supercritical regime. PBHs formed in the two regimes might obey different power laws, and the transition region could just be the peak at $\sim 30M_{\odot}$ seen by LIGO-Virgo. We shall first briefly describe how these black holes are formed, and then discuss how they are constrained by observations including LIGO-Virgo.

A. PBH formation

Vacuum bubbles could nucleate during inflation via quantum tunneling if there is a (positive) “true” vacuum near the inflationary (quasi-de Sitter) vacuum in a multidimensional

field potential. The bubble interior has an energy density ρ_b smaller than the inflationary energy density ρ_i . A typical bubble expands rapidly, almost at the speed of light. After inflation ends, inflatons outside the bubble turn into radiation with density $\rho_r \approx \rho_i$, and the bubble will run into the surrounding radiation fluid with a huge Lorentz factor. The bubble continues to grow, but will eventually come to a halt with respect to the Hubble flow, because all the forces acting on the bubble wall, including the interior vacuum pressure, exterior radiation pressure, and the wall's surface tension, point inwards. A bubble is called “subcritical” if it simply collapses into a black hole after reentering the Hubble horizon. A supercritical bubble, on the other hand, will inflate without bound due to the repulsive vacuum inside. However, instead of consuming our universe, the bubble grows into a baby universe, which is connected to us by a wormhole. For an exterior observer, the wormhole is a spherical object that will eventually turn into a black hole as the “throat” pinches off. Once the relation between the black hole mass in these two regimes and the bubble's size at the end of inflation is determined, we are able to obtain the mass spectrum of these black holes from the bubbles' size distribution.

In ref. [26], we considered an ideal scenario where radiation outside the bubble can be completely reflected by the bubble wall, which implies strong interactions between the bubble field and the standard model particles. In this setting, the mass function was found to be $f \propto m^{-1/2}$ in the supercritical regime. As we know from the previous section, such a distribution is disfavored by the LIGO-Virgo results.

In ref. [27], we studied the other extreme possibility, where the bubble wall is transparent, and radiation can freely flow inside. In this case, the trajectory of the bubble wall before it ceases to grow with respect to the Hubble flow can be estimated by assuming an FRW metric dominated by radiation outside the bubble and matching the spacetimes on two sides of the wall. Let r be the the bubble's comoving radius. The equation of motion of the bubble wall can be found to be

$$\ddot{r} + (4 - 3a^2\dot{r}^2) H\dot{r} + \frac{2}{a^2r} (1 - a^2\dot{r}^2) + \left(\frac{\rho_b}{\sigma} + 6\pi\sigma\right) \frac{(1 - a^2\dot{r}^2)^{3/2}}{a} = 0, \quad (17)$$

where the overdot represents the derivative with respect to cosmic time t , $H \equiv \dot{a}/a = (2t)^{-1}$ is the Hubble parameter in the exterior FRW universe, and σ is the surface tension of the bubble wall. Let t_i be the time when inflation ends, then the scale factor is defined by $a = (t/t_i)^{1/2}$. The “initial” conditions of eq. (17) is $r(t_i) = r_i$ and $\dot{r}(t_i) = (1 - \gamma_i^{-2})^{1/2}$,

where r_i can be smaller or much larger than the Hubble horizon H_i^{-1} at t_i , and γ_i (regarded as a free parameter²) is the Lorentz factor of the bubble wall with respect to the Hubble flow at t_i .

Assuming a huge γ_i , the trajectory of the wall can be approximated by $ar \approx 1$. Let t_s be the time when the wall comes to a stop with respect to the Hubble flow. The bubble's comoving radius at t_s can then be estimated as

$$r_s \equiv r(t_s) \sim r_i + (a_s - 1) H_i^{-1}, \quad (18)$$

where $a_s \equiv (t_s/t_i)^{1/2}$. We are particularly interested in the case where γ_i is so large that $r_s \gg r_i$. In this case, $r_s \sim a_s H_i^{-1}$, and hence the bubble's physical radius at t_s can be estimated as

$$R_s \equiv a_s r_s \sim a_s^2 H_i^{-1} \sim t_s, \quad (19)$$

which means the bubble size is comparable to the Hubble horizon at t_s .

1. *subcritical bubble*

A bubble with sufficiently small r_i would continue to expand after t_s , until it reaches a maximum physical size R_{max} . It will then shrink and eventually collapse into a black hole. By eq. (19), the bubble reenters the horizon at $\sim t_s$, then its evolution will no longer be affected by Hubble expansion significantly, which means the mass of the bubble itself (excluding radiation inside) will almost conserve after then. When the bubble radius reaches R_{max} , the kinetic energy of the bubble wall vanishes. Furthermore, since the bubble is expected to shrink upon horizon reentry, we have $R_{max} \sim R_s$. Hence, the mass of the resulting black hole from a subcritical bubble is

$$m \sim \frac{4}{3}\pi\rho_b R_s^3 + 4\pi\sigma R_s^2 - 8\pi^2\sigma^2 R_s^3. \quad (20)$$

Here the three terms can be understood as the volume energy, the surface energy and the surface binding energy, respectively.

As r_i is increased to a critical value, R_{max} can no longer be reached, because a sufficiently large bubble dominated by its interior vacuum would inflate. When this happens, we enter the supercritical regime.

² See discussion in section IV.

2. supercritical bubble

Due to the third term on the left hand side in eq. (17), a bubble with a larger r_i experiences a smaller “friction” as it grows, and therefore has a larger t_s . By the time t_s , the bubble’s vacuum density ρ_b could become even larger than the exterior radiation density $\rho_r(t_s)$ (note that $\rho_r(t_i) = \rho_i > \rho_b$), i.e.,

$$\rho_r(t_s) = \rho_i a_s^{-4} \lesssim \rho_b. \quad (21)$$

Then by eq. (19),

$$R_s \sim a_s^2 H_i^{-1} = \left(\frac{8\pi}{3} \rho_i a_s^{-4} \right)^{-1/2} \gtrsim \left(\frac{8\pi}{3} \rho_b \right)^{-1/2} = H_b^{-1}. \quad (22)$$

Here H_b^{-1} is the de Sitter horizon associated with the bubble vacuum. $R_s \gtrsim H_b^{-1}$ then implies that the bubble would inflate before t_s and thus create a wormhole, which later turns into a black hole. By the estimate in ref. [27], the black hole mass in this supercritical regime is

$$m \sim H_i (r_s - c_s a_s H_i^{-1})^2, \quad (23)$$

where c_s is the speed of sound in the radiation fluid, and the value of a_s is determined by solving eq. (17). By the estimate in eq. (19), we have $m \sim H_i r_s^2 \sim a_s^2 H_i^{-1} \approx t_s$, which is the horizon mass at t_s .

Therefore, by numerically integrating eq. (17) till $\dot{r} = 0$, we are able to find out the black hole masses in the subcritical and the supercritical regimes. These two regimes are expected to be connected by a region where the black hole mass transits smoothly from one regime to the other. In practice, we evaluate both (20) and (23), and take the smaller one to be the black hole mass for a certain bubble.

B. Size distribution and mass function

Now that we have the masses of black holes from bubbles with various r_i , we need the distribution of r_i in order to obtain the mass function. Bubbles formed earlier expand to larger sizes, but they are rarer due to cosmic expansion. By assuming that bubbles are formed with a vanishing size and that the bubble worldsheet is the future light cone of the

nucleation point, one can find the number density of bubbles having radius in the interval $(r_i, r_i + dr_i)$ at t ($t > t_i$) to be [25]

$$dn(t) \approx \lambda \frac{dr_i}{a(t)^3 (r_i + H_i^{-1})^4}. \quad (24)$$

where λ is the dimensionless bubble nucleation rate per Hubble volume per Hubble time. Then by the definition of $f(m)$ (eqs. (1) and (3)), we have

$$f(m) \propto \frac{\lambda m^2}{H_i^{3/2} (r_i + H_i^{-1})^4} \frac{dr_i}{dm}. \quad (25)$$

The relation between r_i and m can be found by numerically solving eq. (17) and using eqs. (20) and (23). Therefore, the mass function is completely determined by the following five (independent) parameters: the Lorentz factor of the bubble wall at the end of inflation γ_i , the bubble nucleation rate λ , the inflationary density ρ_i , the vacuum density of the bubble interior ρ_b , and the bubble wall tension σ . In the following we shall use

$$\eta_i \sim \rho_i^{1/4}, \quad \eta_b \sim \rho_b^{1/4}, \quad \eta_\sigma \sim \sigma^{1/3}, \quad (26)$$

to characterize ρ_i , ρ_b and σ . They represent the energy scales of inflation, bubble interior and bubble wall, respectively.

Depending on the parameter values, the mass function (25) can have very different shapes and can be wide or relatively narrow. Several examples of $f(m)$ are shown in fig. 4, where we have fixed all other parameters except for the Lorentz factor γ_i .³ An intriguing feature relevant to our discussion is that when γ_i is sufficiently large, black holes in the supercritical regime near the transition approximately follow a power law $f(m) \propto m^{-4}$ (by a numerical fit to the curves)⁴, which is what LIGO-Virgo implies for PBHs with $m > m_* \sim 35M_\odot$. Moreover, there is a peak in the transition region for some values of γ_i , and the mass function can be approximated by different power laws on two sides of the peak. Now the question is whether suitable bubble parameters can be found such that subcritical black holes obeys $f(m) \propto m^{1.2}$.

³ Note that other parameters are not less essential than γ_i . Varying them will give different curves of $f(m)$ (shifting positions on the f - m plane) that look similar to those in fig. 4.

⁴ A semi-analytic discussion of this relation can be found in the appendix. For supercritical bubbles with a huge γ_i , the mass function near the transition satisfies $f \propto m^{-4.25}$.

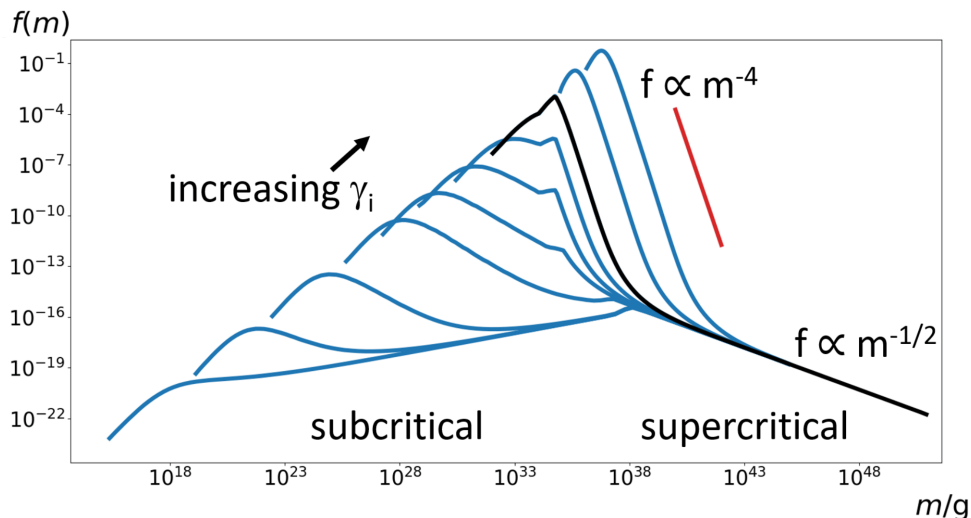


FIG. 4: Some examples of the mass function $f(m)$ given by (25). We have fixed parameters except for the Lorentz factor γ_i , with $\lambda \approx 10^{-21}$, $\eta_i \approx 10^{-16} M_{Pl}$, $\eta_b \approx 6 \times 10^{-21} M_{Pl}$, $\eta_\sigma \approx 4 \times 10^{-15} M_{Pl}$, and γ_i varying from 10^4 to 10^{30} . For small γ_i the maximum of $f(m)$ appears at the transition region. As γ_i increases, another peak develops in the subcritical regime. For a sufficiently large γ_i , supercritical black holes near the transition region approximately follow a power law $f \propto m^{-4}$ (the red straight line is $\propto m^{-4}$). For large masses, all spectra approach $f \propto m^{-1/2}$. The mass function in black (the third one from the right) agrees well with the broken power law suggested by LIGO in the relevant mass range, as shown in fig. 5.

C. Observational constraints

The answer is yes. In fact, there are many sets of bubble parameters that can give the desired mass function. In fig. 5 we show an example of $f(m)$ with $\gamma_i \approx 10^{22}$, $\lambda \approx 10^{-21}$, $\eta_i = \mathcal{O}(1)$ TeV, $\eta_b = \mathcal{O}(0.1)$ GeV and $\eta_\sigma = \mathcal{O}(10)$ TeV (black, solid curve). It agrees well with the broken power law mass function with the parameters in eq. (14) (orange, dashed lines). As a comparison, we also show the best-fit log-normal function (green, dotted curve). The light grey and colored areas are regions excluded by different astrophysical observations (see ref. [33] for a recent review). Strictly speaking, these upper bounds are valid only for PBHs with a very narrow spectrum, and so are not supposed to be used to compare with an extended mass function $f(m)$. (The method of applying these bounds on a broad spectrum was discussed in ref. [34].) Loosely speaking, however, as long as $\psi(m) = f(m)/m$ does not

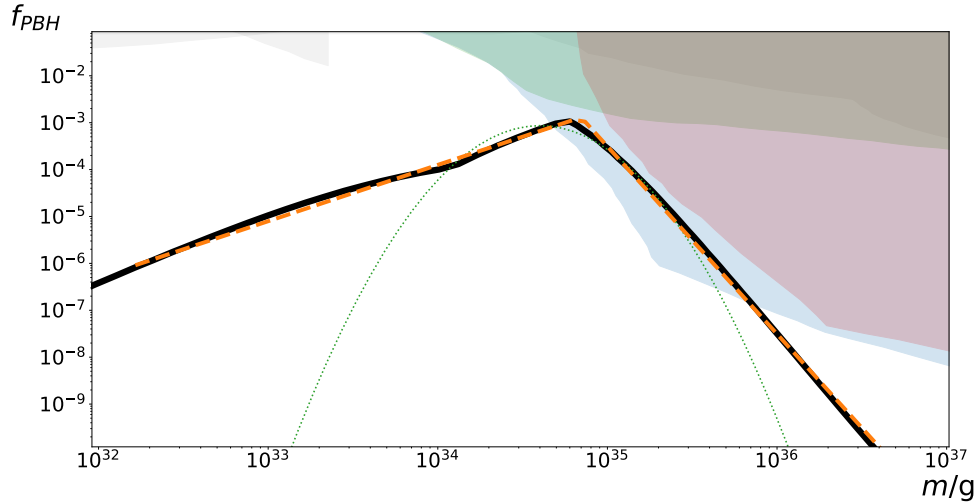


FIG. 5: Observational constraints on our mechanism. The light grey, light blue and light purple regions are excluded for PBHs with a monochromatic spectrum [35, 40–44] (adapted from fig. 10 in ref. [33]). The light green region is a modification of the light blue, with the effect of PBH accretion taken into account [36]. The black solid curve is a possible distribution from our PBH mechanism. The orange dashed lines are the best-fit broken power law, with $f \propto m^{1.2}$ for $m < 35M_{\odot}$ and $f \propto m^{-4}$ for $m > 35M_{\odot}$. The green dotted curve is the best-fit log-normal mass function.

have a plateau over a relatively big range, we can still constrain a model by placing $f(m)$ near the bounds while avoiding hitting them.

The most stringent bound for us in fig. 5, which covers the mass range around $30\text{--}300M_{\odot}$, comes from Planck. Ref. [35] studied how disk or spherical accretion of a halo around PBHs could affect CMB, which strongly constrains the population of PBHs in the range around $1\text{--}10^4M_{\odot}$. The broken power law function implied by LIGO-Virgo seems in tension with the model of disk accretion (light blue), but is free from the bound imposed by spherical accretion (light purple). However, we note that the effect of PBH accretion was not taken into account in our discussion. It is pointed out in refs. [36–38] that efficient PBH accretion before the reionization epoch tends to relax the tension with these bounds.⁵ For instance,

⁵ Although the process of PBH accretion is model-dependent, and is even more uncertain for binary systems, it is generally agreed that PBHs with masses smaller than $\mathcal{O}(10)M_{\odot}$ are not significantly affected by accretion, and so have tiny spins, while larger PBHs generally have larger spins. This is compatible with the LIGO-Virgo results that the correlation between mass and the mean effective spin is negative, whereas the correlation between mass and the spin dispersion is positive [39]. The best-fit of a one-parameter

if one adopts the one-parameter (denoted by $z_{\text{cut-off}}$) accretion model in ref. [36] (here with $z_{\text{cut-off}} = 10$), the light blue constraint in fig. 5 is relaxed to the light green region, which does not intersect with our mass function.

Besides being able to account for the LIGO-Virgo black holes, another interesting feature of our mass function is that it may provide an explanation to supermassive black holes (SMBHs) at the center of most galaxies [45, 46]. These black holes have masses from $\sim 10^6\text{--}10^{10}M_\odot$, which cannot be explained by standard accretion models [47]. Moreover, observations of quasars indicate that many of them were already in place at high redshifts (see ref. [48] for a review). Recently, a black hole as large as $\sim 10^9M_\odot$ was discovered at $z \approx 7.6$, which greatly challenges the conventional formation theory of astrophysical black holes [49]. One is then led to speculate that SMBHs were seeded by PBHs, which could have large masses by birth [19, 50–53]. At the present time (t_0), the number density of PBHs of mass $\sim m$ is approximately given by

$$n(m) \sim \rho_{CDM}(t_0) \frac{f(m)}{m} \approx 4 \times 10^{11} \left(\frac{M_\odot}{m} \right) f(m) \text{ Mpc}^{-3}. \quad (27)$$

It was shown in refs. [35] that PBHs at $z \sim 6$ with $m \sim 10^2\text{--}10^4M_\odot$ can attain sufficient accretion and grow to SMBHs even if $f(m)$ is as small as 10^{-9} . We can see from fig. 5 that the best-fit broken power law mass function gives $f(10^3M_\odot) \gtrsim 10^{-9}$, which gives $n(10^3M_\odot) \sim 0.4 \text{ Mpc}^{-3}$. This is larger than the present density of galaxies $\sim 0.1 \text{ Mpc}^{-3}$. Therefore, SMBHs could indeed have been seeded by these PBHs.

IV. CONCLUSIONS AND DISCUSSION

In this work we have used maximum likelihood estimation to analyze the GWTC-1 and GWTC-2 datasets released by the LIGO-Virgo Collaboration, assuming that all of the black holes in the 44 confident merger events are PBHs with a mass spectrum $f(m)$ satisfying a broken power law. We found that the best-fit $f(m)$ has a peak at $m_* \approx 35M_\odot$, consistent with the observations, and that $f \propto m^{1.2}$ for $m < m_*$ and $f \propto m^{-4}$ for $m > m_*$. These black holes can constitute about 0.1% of the dark matter.

Such a unique mass function can be realized in a mechanism of PBH formation we proposed in recent years, where the black holes are formed by vacuum bubbles that could

accretion model with the GWTC-1 and GWTC-2 catalogs can be found in ref. [24].

nucleate during inflation. In general, the inflaton field rolls in a multidimensional potential containing a number of minima. Bubble nucleation can occur during inflation if a minimum has energy scale lower than the inflationary scale. After inflation ends, depending on their size, these bubbles will turn into black holes either by simple collapse (subcritical), or by creating a wormhole (supercritical). The resulting mass function of the black holes may obey different power laws in the two regimes, which are connect by a transition region that could possibly be at m_* . Surprisingly, if the bubble walls have a sufficiently large Lorentz factor at the end of inflation, which is typically the case, the mass function in the supercritical regime near m_* is indeed approximately given by $f \propto m^{-4}$. With properly chosen parameters (including the Lorentz factor, the energy scales of bubble vacuum, bubble wall and inflation), we can have $f \propto m^{1.2}$ for $m < m_*$.

With this mass function, we can also have a sufficient number of seeds ($m \sim 10^3 M_\odot$) that could grow into SMBHs observed at the galactic centers, which is difficult to explain with conventional accretion models. In addition, as we can see in fig. 4, it is also possible to estimate the distribution of stupendously large black holes [54] from the large mass end, where $f \propto m^{-1/2}$. This however will not be discussed further in the present work.

Another noticeable feature of our mass function is that it suggests a relatively low inflationary scale. During the slow roll, the ultimate Lorentz factor of the bubble wall for a comoving observer outside the bubble is $\gamma \sim \eta_i^2 M_{Pl} / \eta_\sigma^{(i)3}$, where $\eta_\sigma^{(i)}$ is the energy scale of the wall tension σ during inflation [27, 55]. We assumed γ to be the Lorentz factor of the wall as it runs into the ambient radiation after inflation, i.e., $\gamma_i = \gamma$. However, at the end of inflation, the inflaton quickly rolls down into our vacuum, which could cause a drastic change in σ since the shape of the barrier in the field potential could change significantly. Therefore, we regarded γ_i and σ as two free parameters. With the parameter values that lead to the black solid mass function in fig. 5, where the inflationary scale is $\eta_i = \mathcal{O}(1)$ TeV, we have $\eta_\sigma / \eta_\sigma^{(i)} = \mathcal{O}(100\text{--}1000)$. If we require a larger η_i , the ratio $\eta_\sigma / \eta_\sigma^{(i)}$ is even larger, which seems less likely. Of course, this should be determined by the configuration of the multidimensional potential, which is beyond the scope of the present work.

An inflationary model at the TeV scale was constructed in ref. [56]. In this model of hybrid inflation, the inflaton is directly coupled to the Higgs field such that the symmetry

is restored even at a temperatures lower than the electroweak scale.⁶ As the Higgs potential becomes unstable later, the fields roll down in random directions, leading to non-trivial Higgs configurations. In the presence of CP-violation, this might produce a baryon asymmetry, which is referred to as cold electroweak baryogenesis [57–60], and has been studied extensively with simulations [61–64]. Such a process might also be a source of primordial magnetic fields [65, 66] and stochastic gravitational waves [67].

In hybrid inflation, the inflationary scale could be so small that the expansion rate is much smaller than the typical particle decay rate, hence thermalization occurs almost instantaneously compared to Hubble time [57]. This is compatible with the assumption in our model where the bubble runs into radiation immediately after inflation ends. If this is not the case, a different matter content during reheating would change the scale factor in the equation of motion of the bubble wall (eq. (17)). To see how this would affect the resulting mass function, we solved the equation assuming the universe is dust-dominated for the first few Hubble times. It turned out the desired mass function (in fig. 5) can be obtained by, e.g., increasing γ_i and η_σ (by a factor $\mathcal{O}(1-10)$) without changing other parameters.

With many more merger events to be detected by LIGO-Virgo in the near future, the mass distribution of black holes can be determined with increasing certainty. Excited as we are, that our mechanism is the only factory of LIGO-Virgo black holes can be ruled out if the mass function turns out to have a very different shape, such as one with a slope (in the log-log plot) much smaller than -4 for large black holes.

Appendix: Mass distribution of supercritical black holes

In this appendix, we will find a semi-analytic solution to the bubble wall’s equation of motion for relatively large bubbles, and thus determine the mass function of supercritical black holes, which was found numerically in section III, and is shown in fig. 4.

The bubble wall’s equation of motion after inflation is (eq. (17))

$$\ddot{r} + (4 - 3a^2\dot{r}^2) H\dot{r} + \frac{2}{a^2r} (1 - a^2\dot{r}^2) + K \frac{(1 - a^2\dot{r}^2)^{3/2}}{a} = 0, \quad (28)$$

⁶ New fields need to be introduced in order to produce bubbles in our model.

where we have defined $K \equiv \rho_b/\sigma + 6\pi\sigma$. This equation can be rewritten as

$$\dot{u} + \frac{3}{2t}u + \frac{2\gamma}{ar} + K = 0, \quad (29)$$

where $u(t) \equiv \sqrt{\gamma^2 - 1}$ and $\gamma \equiv (1 - a^2\dot{r}^2)^{-1/2}$. As discussed in section III, if we assume a huge γ_i (or $u(t_i)$), the trajectory of the wall can be approximated by $a\dot{r} \approx 1$, which gives

$$r(t) \approx r_i + 2\sqrt{t_i}(\sqrt{t} - \sqrt{t_i}). \quad (30)$$

Then when the wall comes to a stop with respect to the Hubble flow, we have

$$r_s \sim r_i + a_s H_i^{-1}, \quad (31)$$

where we have used $r_i \gg H_i^{-1}$, which is typically the case for supercritical bubbles in our discussion. In what follows we shall discuss two limits: (a) $r_i \gg a_s H_i^{-1}$, and (b) $r_i \ll a_s H_i^{-1}$.

$$(a) \ r_i \gg a_s H_i^{-1}$$

In this limit, $r_s \sim r_i$. Then by eq. (23), the resulting black hole mass is

$$m \propto r_i^2. \quad (32)$$

Then it can easily be shown that the mass function (eq. (25)) becomes

$$f(m) \propto \frac{m^2}{r_i^4} \frac{dr_i}{dm} \propto m^{-1/2}. \quad (33)$$

This explains the behavior of $f(m)$ on the end of large masses, as shown in fig. 4.

$$(b) \ r_i \ll a_s H_i^{-1}$$

In this limit, the bubbles are assumed to still be in the supercritical regime, but their initial radius r_i is negligible compared to $r_s \sim a_s H_i^{-1}$. By eq. (30), we can approximate eq. (29) by

$$\dot{u} + \frac{3}{2t}u + \frac{2u}{r_i\sqrt{t}/\sqrt{t_i} + 2t} + K = 0. \quad (34)$$

Now we can roughly divide the time interval between t_i and t_s by two stages: before and after $t \approx r_i^2/4t_i \equiv t_m$, which determines whether $r_i\sqrt{t}/\sqrt{t_i}$ or $2t$ dominates the denominator in the third term of the above equation.

Before t_m , we have

$$\dot{u} + \frac{3}{2t}u + \frac{2\sqrt{t_i}}{r_i\sqrt{t}}u + K = 0, \quad (35)$$

which has an analytic solution

$$u(t) = \frac{e^{-4\sqrt{t_i t}/r_i}}{t^{3/2}} \left[\frac{\gamma_i t_i^{3/2}}{e^{-4t_i/r_i}} + K \frac{\Gamma(5, -4t_i/r_i) - \Gamma(5, -4\sqrt{t_i t}/r_i)}{512(\sqrt{t_i}/r_i)^5} \right]. \quad (t < t_m) \quad (36)$$

Here we have taken into account the initial condition $u(t_i) = \gamma_i$. Then at t_m , we have

$$u(t_m) = \frac{e^{-2}}{t_m^{3/2}} \left[\frac{\gamma_i t_i^{3/2}}{e^{-4t_i/r_i}} + K \frac{\Gamma(5, -4t_i/r_i) - \Gamma(5, -2)}{512(\sqrt{t_i}/r_i)^5} \right] \quad (37)$$

After t_m , eq. (34) becomes

$$\dot{u} + \frac{5}{2t}u + K = 0, \quad (38)$$

with the solution

$$u(t) = u(t_m) \left(\frac{t_m}{t} \right)^{5/2} + \frac{2}{7} K t \left[\left(\frac{t_m}{t} \right)^{7/2} - 1 \right]. \quad (t > t_m) \quad (39)$$

At t_s , we have $u(t_s) = 0$. After some algebra, substituting $u(t_m)$ by eq. (37) in eq. (39) leads to

$$t_s \approx 0.5 \left(\frac{\gamma_i}{K} \right)^{2/7} t_i^{1/7} r_i^{4/7}. \quad (40)$$

In the computations we have assumed the relation $\gamma_i > 10^{-3} K r_i^5 / t_i^4$, which is true in the cases we are interested in. This estimate for t_s has also been verified numerically.

Now by eq. (23), we have

$$m \sim t_s \propto r_i^{4/7}. \quad (41)$$

Then the mass function becomes

$$f(m) \propto \frac{m^2}{r_i^4} \frac{dr_i}{dm} \propto m^{-4.25}. \quad (42)$$

This explains the behavior of $f(m)$ in the supercritical regime near the transition, as shown in fig. 4. Note that this relation is but an approximation. For a smaller γ_i , it was numerically found that the power for m gets slightly larger, giving $f \propto m^{-4}$, as shown in fig. 5.

Acknowledgments

I would like to thank Tanmay Vachaspati, Ville Vaskonen, Alex Vilenkin and the anonymous referee for stimulating discussion and comments. This work is supported by the U.S. Department of Energy, Office of High Energy Physics, under Award No. de-sc0019470 at Arizona State University.

-
- [1] B. P. Abbott et al. (LIGO Scientific, Virgo), *Phys. Rev. X* **9**, 031040 (2019), 1811.12907.
 - [2] R. Abbott et al. (LIGO Scientific, Virgo) (2020), 2010.14527.
 - [3] K. W. K. Wong, K. Breivik, K. Kremer, and T. Callister (2020), 2011.03564.
 - [4] M. Zevin, S. S. Bavera, C. P. L. Berry, V. Kalogera, T. Fragos, P. Marchant, C. L. Rodriguez, F. Antonini, D. E. Holz, and C. Pankow (2020), 2011.10057.
 - [5] C. L. Rodriguez, K. Kremer, S. Chatterjee, G. Fragione, A. Loeb, F. A. Rasio, N. C. Weatherford, and C. S. Ye (2021), 2101.07793.
 - [6] M. Fishbach, Z. Doctor, T. Callister, B. Edelman, J. Ye, R. Essick, W. M. Farr, B. Farr, and D. E. Holz (2021), 2101.07699.
 - [7] S. Bird, I. Cholis, J. B. Muñoz, Y. Ali-Haïmoud, M. Kamionkowski, E. D. Kovetz, A. Racanelli, and A. G. Riess, *Phys. Rev. Lett.* **116**, 201301 (2016), 1603.00464.
 - [8] S. Clesse and J. García-Bellido, *Phys. Dark Univ.* **15**, 142 (2017), 1603.05234.
 - [9] M. Sasaki, T. Suyama, T. Tanaka, and S. Yokoyama, *Phys. Rev. Lett.* **117**, 061101 (2016), 1603.08338.
 - [10] M. Raidal, V. Vaskonen, and H. Veermäe, *JCAP* **09**, 037 (2017), 1707.01480.
 - [11] Y. Ali-Haïmoud, E. D. Kovetz, and M. Kamionkowski, *Phys. Rev. D* **96**, 123523 (2017), 1709.06576.
 - [12] V. Vaskonen and H. Veermäe, *Phys. Rev. D* **101**, 043015 (2020), 1908.09752.
 - [13] J. Garriga and N. Triantafyllou, *JCAP* **09**, 043 (2019), 1907.01455.
 - [14] M. Raidal, C. Spethmann, V. Vaskonen, and H. Veermäe, *JCAP* **02**, 018 (2019), 1812.01930.
 - [15] Z.-C. Chen and Q.-G. Huang, *Astrophys. J.* **864**, 61 (2018), 1801.10327.
 - [16] A. D. Gow, C. T. Byrnes, A. Hall, and J. A. Peacock, *JCAP* **01**, 031 (2020), 1911.12685.
 - [17] Y. Wu, *Phys. Rev. D* **101**, 083008 (2020), 2001.03833.

- [18] A. Dolgov and J. Silk, Phys. Rev. D **47**, 4244 (1993).
- [19] S. Clesse and J. García-Bellido, Phys. Rev. D **92**, 023524 (2015), 1501.07565.
- [20] S. Blinnikov, A. Dolgov, N. K. Porayko, and K. Postnov, JCAP **11**, 036 (2016), 1611.00541.
- [21] K. Kannike, L. Marzola, M. Raidal, and H. Veermäe, JCAP **09**, 020 (2017), 1705.06225.
- [22] G. Hütsi, M. Raidal, V. Vaskonen, and H. Veermäe (2020), 2012.02786.
- [23] A. Hall, A. D. Gow, and C. T. Byrnes, Phys. Rev. D **102**, 123524 (2020), 2008.13704.
- [24] K. W. K. Wong, G. Franciolini, V. De Luca, V. Baibhav, E. Berti, P. Pani, and A. Riotto (2020), 2011.01865.
- [25] J. Garriga, A. Vilenkin, and J. Zhang, JCAP **1602**, 064 (2016), 1512.01819.
- [26] H. Deng and A. Vilenkin, JCAP **1712**, 044 (2017), 1710.02865.
- [27] H. Deng, JCAP **09**, 023 (2020), 2006.11907.
- [28] M. Dominik, E. Berti, R. O’Shaughnessy, I. Mandel, K. Belczynski, C. Fryer, D. E. Holz, T. Bulik, and F. Pannarale, Astrophys. J. **806**, 263 (2015), 1405.7016.
- [29] P. Ajith et al., Phys. Rev. D **77**, 104017 (2008), [Erratum: Phys.Rev.D 79, 129901 (2009)], 0710.2335.
- [30] I. Mandel, W. M. Farr, and J. R. Gair, Mon. Not. Roy. Astron. Soc. **486**, 1086 (2019), 1809.02063.
- [31] H. Deng, J. Garriga, and A. Vilenkin, JCAP **04**, 050 (2017), 1612.03753.
- [32] V. De Luca, G. Franciolini, and A. Riotto, Phys. Lett. B **807**, 135550 (2020), 2001.04371.
- [33] B. Carr, K. Kohri, Y. Sendouda, and J. Yokoyama (2020), 2002.12778.
- [34] B. Carr, M. Raidal, T. Tenkanen, V. Vaskonen, and H. Veermäe, Phys. Rev. **D96**, 023514 (2017), 1705.05567.
- [35] P. D. Serpico, V. Poulin, D. Inman, and K. Kohri, Phys. Rev. Res. **2**, 023204 (2020), 2002.10771.
- [36] V. De Luca, G. Franciolini, P. Pani, and A. Riotto, Phys. Rev. D **102**, 043505 (2020), 2003.12589.
- [37] V. De Luca, V. Desjacques, G. Franciolini, P. Pani, and A. Riotto, Phys. Rev. Lett. **126**, 051101 (2021), 2009.01728.
- [38] V. De Luca, G. Franciolini, P. Pani, and A. Riotto, JCAP **06**, 044 (2020), 2005.05641.
- [39] M. Safarzadeh, W. M. Farr, and E. Ramirez-Ruiz, Astrophys. J. **894**, 129 (2020), 2001.06490.
- [40] C. Alcock et al. (MACHO), Astrophys. J. **542**, 281 (2000), astro-ph/0001272.

- [41] P. Tisserand et al. (EROS-2), *Astron. Astrophys.* **469**, 387 (2007), astro-ph/0607207.
- [42] M. Oguri, J. M. Diego, N. Kaiser, P. L. Kelly, and T. Broadhurst, *Phys. Rev. D* **97**, 023518 (2018), 1710.00148.
- [43] B. P. Abbott et al. (LIGO Scientific, Virgo), *Phys. Rev. Lett.* **123**, 161102 (2019), 1904.08976.
- [44] Y. Inoue and A. Kusenko, *JCAP* **10**, 034 (2017), 1705.00791.
- [45] D. Lynden-Bell, *Nature* **223**, 690 (1969).
- [46] J. Kormendy and D. Richstone, *Ann. Rev. Astron. Astrophys.* **33**, 581 (1995).
- [47] Z. Haiman, *Astrophys. J.* **613**, 36 (2004), astro-ph/0404196.
- [48] J. Kormendy and L. C. Ho, *Ann. Rev. Astron. Astrophys.* **51**, 511 (2013), 1304.7762.
- [49] F. Wang, J. Yang, X. Fan, J. F. Hennawi, A. J. Barth, E. Banados, F. Bian, K. Boutsia, T. Connor, F. B. Davies, et al., *The Astrophysical Journal Letters* **907**, L1 (2021).
- [50] S. G. Rubin, A. S. Sakharov, and M. Yu. Khlopov, *J. Exp. Theor. Phys.* **91**, 921 (2001), [*J. Exp. Theor. Phys.*92,921(2001)], hep-ph/0106187.
- [51] R. Bean and J. Magueijo, *Phys. Rev.* **D66**, 063505 (2002), astro-ph/0204486.
- [52] N. Duechting, *Phys. Rev.* **D70**, 064015 (2004), astro-ph/0406260.
- [53] B. Carr and J. Silk, *Mon. Not. Roy. Astron. Soc.* **478**, 3756 (2018), 1801.00672.
- [54] B. Carr, F. Kuhnel, and L. Visinelli, *Mon. Not. Roy. Astron. Soc.* **501**, 2 (2021), 2008.08077.
- [55] V. Berezin, V. Kuzmin, and I. Tkachev, *Phys. Rev. D* **36**, 2919 (1987).
- [56] E. J. Copeland, D. Lyth, A. Rajantie, and M. Trodden, *Phys. Rev. D* **64**, 043506 (2001), hep-ph/0103231.
- [57] J. Garcia-Bellido, D. Y. Grigoriev, A. Kusenko, and M. E. Shaposhnikov, *Phys. Rev. D* **60**, 123504 (1999), hep-ph/9902449.
- [58] L. M. Krauss and M. Trodden, *Phys. Rev. Lett.* **83**, 1502 (1999), hep-ph/9902420.
- [59] J. Smit and A. Tranberg, in *5th International Conference on Strong and Electroweak Matter* (2003), pp. 509–513, hep-ph/0210348.
- [60] T. Konstandin and G. Servant, *JCAP* **07**, 024 (2011), 1104.4793.
- [61] A. Tranberg and J. Smit, *JHEP* **08**, 012 (2006), hep-ph/0604263.
- [62] A. Tranberg, J. Smit, and M. Hindmarsh, *JHEP* **01**, 034 (2007), hep-ph/0610096.
- [63] Z.-G. Mou, P. M. Saffin, and A. Tranberg, *JHEP* **07**, 010 (2017), 1703.01781.
- [64] Z.-G. Mou, P. M. Saffin, and A. Tranberg, *JHEP* **05**, 197 (2018), 1803.07346.
- [65] A. Diaz-Gil, J. Garcia-Bellido, M. Garcia Perez, and A. Gonzalez-Arroyo, *JHEP* **07**, 043

(2008), 0805.4159.

[66] Z.-G. Mou, P. M. Saffin, and A. Tranberg, *JHEP* **06**, 075 (2017), 1704.08888.

[67] J. Garcia-Bellido, D. G. Figueroa, and A. Sastre, *Phys. Rev. D* **77**, 043517 (2008), 0707.0839.